J Mater Sci: Mater Electron (2014) 25:2210–2219
DOI 10.1007/s10854-014-1861-y

AlN epilayers and nanostructures growth in a homebuilt alumina hot-wall high temperature chemical vapor deposition system

Dian Zhang · Fa-Min Liu · Yuan Yao · Xin-An Yang

Received: 25 December 2013 / Accepted: 4 March 2014 / Published online: 12 March 2014
© Springer Science+Business Media New York 2014

Abstract AlN epilayers and nanostructures were grown in the range from 500 to 1500 °C in a homebuilt alumina hot-wall high temperature chemical vapor deposition system. The results revealed that high quality AlN epilayers can be grown at high temperature beyond 1100 °C and versatile AlN nanostrctures can be grown at low temperature below 900 °C, enabling the system to tailor AlN structures just by changing the growth temperature. High growth temperature as well as low N/Al ratio was preferable to surface mobility of the adatoms and lateral growth, resulting in a series of morphology changes. Meanwhile, the crystal quality improved with the increasing growth temperature, as proved by the decreasing FWHM of (0002) plane rocking curve of the epilayer and narrowing peaks in θ-2θ XRD pattern of the nanostructures. The epitaxial relationship was proven to be AlN (0001) || sapphire (0001) and AlN [1-210] || sapphire [1-100]. The layer was in tensile stress state in several tens of nanometers range near the interface and turned into compressive stress state out of the range. Tens of atoms layers of sapphire interface were substituted for AlN lattice due to nitridation. Low growth temperature produced versatile AlN nanostructures, whose crystal structures varied from amorphous in 500 °C case to defective crystal in 700 °C case and improved crystallinity in 900 °C case.

D. Zhang · F.-M. Liu (✉)
Department of Physics, School of Physics and Nuclear Energy Engineering, Beihang University, Beijing 100191, China
e-mail: fmliu@buaa.edu.cn

Y. Yao · X.-A. Yang
Beijing National Laboratory for Condensed Matter Physics, Institute of Physics, Chinese Academy of Sciences, Beijing 100190, China

1 Introduction

Inspired by the boom of GaN-based optoelectronic devices, many researchers focus their interests on AlN which possesses the widest direct bandgap of 6.2 eV in III-nitrides, whose alloy has bandgap ranged from 1.7 to 6.2 eV [1, 2]. It is ideal substrate material for high-power and high-frequency electronic devices thanks to its excellent thermal conductivity and dielectric properties [3, 4]. Furthermore, it has promising application in surface acoustic wave (SAW) devices [5, 6], micro and nano electro machanical systems (MEMS and NEMS) due to its high acoustic velocity and piezoelectric properties [7, 8]. The most attraction of AlN is its perspective in light emitting diode (LED), laser diode (LD) and detector working at extreme short wavelength around 200 nm [9–11]. Meanwhile, what activates the ambition of crystal growth researchers is that AlN is ideal wafer for other III–V optoelectronic devices, owing to not only the compatibility of their lattice and thermal expansion coefficient but also the transparency of AlN in UV range [12, 13]. In all these applications, AlN crystal growth or layer deposition is fundamental step.

AlN epitaxial layer is generally grown by molecular beam epitaxy (MBE) [14, 15], metal organic chemical vapor deposition (MOCVD) or metal organic vapor phase epitaxy (MOVPE) [12, 16, 17]. To obtain native wafer, AlN bulk single crystal and its boule have been grown via sublimation–recondensation method (SR) or called physical vapor transport (PVT) method by several groups and commercial companies [18–20]. There are also some researchers who grow bulk AlN in solutions [21, 22]. Another attractive method called hydride vapor phase epitaxy (HVPE) was applied for both AlN epilayer [23, 24] and free-standing wafer [25, 26] growth because of its advantages of economic effect, high growth rate and ability of large scale wafer preparation. However, the major disadvantage of

conventional HVPE was its growth temperature limitation of 1200 °C which degrades the crystal quality of the layer [25]. Moreover, the quartz reactor faces the danger of corrosion by hot HCl gas and Al metal [25–27]. In the past several years, continuous efforts were made to overcome the above-mentioned obstacles in HVPE. In order to circumvent the deleterious reactions, Yoshinao Kumagai [25] proposed low source zone temperature of 500 °C to suppress AlCl species that attack the tube violently. Ken-ichi Eriguchi [28, 29] used solid $AlCl_3$ as well as D. F. Bliss [30] adopted solid adduct as Al source in conventional HVPE. To break through the growth temperature limitation of quartz reactor, Jumpei Tajima [31] and Toru Nagashima [25] directly heat substrate by susceptor, as well as Ken-ichi Eriguchi [29] and Jie-Jun Wu [32] applied high power lamp as heater, to obtain high growth temperature of about 1450 °C.

In comparison with HVPE, the chemical vapor deposition (CVD) of AlN film based on the similar process in principle except that it uses solid $AlCl_3$ as Al source. However, although quit a few researches about AlN CVD were fulfilled, the products usually were polycrystalline film instead of epilayer [33, 34]. Even then, CVD was still an attractive and potential method for AlN layer epitaxy as well as nanostructures growth [35–37]. It can fulfill AlN growth without use of dangerous H_2 carrier and chlorides source. Meanwhile, CVD was suitable for mass production because of its simple system and low cost.

In this paper, we established a hot-wall high temperature chemical vapor deposition (HTCVD) system with three zones based on traditional alumina tubular resistance thermal furnace. It can conduct high temperature growth up to 1600 °C to enhance surface mobility of adatoms and reduce content of Al_2Cl_6 species, leading to promotion of the layer quality and the growth rate [28]. Furthermore, all hardware in the furnace was made from high purity sintered alumina which can eliminate deleterious reaction. Besides, the system used Ar carrier and solid $AlCl_3$ source instead of H_2 carrier and HCl or Cl_2 source gas. In addition, the system ran in atmospheric pressure without high vacuum, inert gas protection and purifier. Therefore, the system was simple, safe, easy to scale up and suitable for mass-production with very low cost. In result, high quality AlN thick epilayers and versatile nanostructures were successfully grown in the system, allowing us to tailor AlN structure in a wide range just by changing the growth temperature.

2 Experimental section

2.1 Building up of the system

The homebuilt hot-wall high temperature chemical vapor deposition system for AlN expitaxy was shown in Fig. 1. The furnace contained three independent controlled temperature zones, i.e., source zone for $AlCl_3$ evaporation, middle zone for $AlCl_3$ vapor being heated to avoid its condensation, growth zone for AlN growth.

All hardware in the furnace was made of alumina (99.7 %), including furnace tube, source tube, inner tube, susceptor and thermal insulator. The inner tube configuration could confine the sources gas flow, improve the uniformity of the mixture, maintain correct local N/Al ratio near the substrate and increase flow rate near the substrates surface via its reduced diameter in comparison with the furnace tube. At the inlet of the inner tube located the susceptor of the substrates, which was about 10 mm away from the $AlCl_3$ nozzle. The NH_3 nozzle was assembled in 30° azimuth angle against $AlCl_3$ nozzle so that NH_3 and $AlCl_3$ mix in front of the substrate. Meanwhile, there was 5 mm distance in horizontal direction between NH_3 nozzle and $AlCl_3$ nozzle in order to eliminate parasitic reaction, which would result in clogging of the $AlCl_3$ nozzle and terminate the growth duration. The thermal insulators were applied to obtain abrupt thermal profile. At the same time, the thermal insulator at the upstream entrance of the furnace acted as brace for source tube. The thermal insulator at the downstream exit of the furnace acted as plug between the furnace tube and inner tube in order that the majority of source gas passed through the inner tube.

In front of the furnace was the gas supplier which was not shown. There were four gas lines, i.e., Ar ambient line, NH_3 source line, Ar dilution line, Ar carrier line. All gases were released from their gas cylinders and control by their rotameters respectively. After that, NH_3 and Ar dilution were mixed in a sealed wide-necked bottle (500 ml in volume), following by feeding into NH_3 source tube. Meanwhile, Ar carrier for $AlCl_3$ and Ar ambient were connected to another two sealed wide-necked bottle, following by feeding into $AlCl_3$ source tube and furnace tube respectively. The wide-necked bottles played the role of buffering the pulse of Ar and NH_3 to obtain accurate flow rate and stable flow field in the growth zone. Behind the furnace was the mechanical pump and exhaust scrubber.

Solid anhydrous $AlCl_3$ (Analytical reagent: 99 %), NH_3 (5N) and Ar (5N) were used as Al source, N source and carrier gas respectively. Sapphire (0001) wafer was cleaved into 10 mm square substrates, following by etching in mixture of 98 % sulphuric acid and phosphoric acid (3:1) at 150 °C for 10 min. Then they were cleaned in ultrasonic bath of ethanol, acetone and deionized water and dried naturally for use.

2.2 Growth procedure

In an experiment run, three substrates labeled as S1, S2 and S3 were placed on the susceptor successively with 1 mm

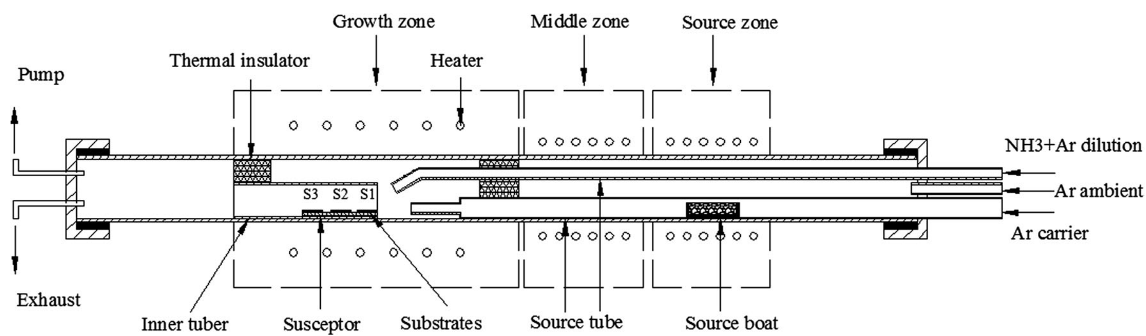

Fig. 1 Sketch of the homebuilt alumina hot-wall high temperature chemical vapor deposition system

spacing along the flow direction, as shown in Fig. 1. Then the inner tube was transferred into the furnace tube and make sure that the S1 substrate was situated at the center of the growth zone. About 5 g anhydrous $AlCl_3$ was loaded in source boat and placed into the source tube. Then the source tubes of NH_3 and $AlCl_3$ were plugged into the furnace tube. Subsequently, the system was sealed up and the growth zone was heated to 150 °C, following by pumping and flushing by Ar flow several times to expel air and moisture. In the case of low temperatures growth, the Ar ambient flow rate was 0.83×10^{-6} m^3/s (50 sccm) during the growth zone was heated up from 150–500 °C, 700 or 900 °C, following by 50 min growth. In the case of high temperature growth, the Ar ambient flow rate was 50 sccm during the growth zone was heated up from 150 to 1050 °C, following by nitridation of the substrates in 50 sccm NH_3. After that, the growth zone was further heated up to 1100 and 1500 °C for 30 min growth as well as to 1300 °C for 50 min growth. In all cases, the temperature of source zone and middle zone were held at 150 and 250 °C respectively during growth. The flow rate of NH_3, Ar carrier of $AlCl_3$ and Ar ambient were fixed at 16.67×10^{-6} m^3/s (1000 sccm) respectively while Ar dilution was shut down. After the growth, the heaters of source zone and middle zone were turned off and the source zone was air cooled to 90 °C in 15 min. Finally, the heater of growth zone was turned off and the furnace was cooled down to room temperature naturally in 0.83×10^{-6} m^3/s (50 sccm) NH_3 and Ar ambient.

2.3 Characterizations

The morphologies and the chemical compositions of the products were studied by FEG XL s 30 scanning electron microscope (SEM) and its affiliated energy dispersive x-ray spectrometer. The products structures were analyzed by Panalytical Empyrean, which had high resolution, Hybrid monochromator, 5-axes cradle and PIXcel detector. The operating voltage of 40 kV and a current of 40 mA, using Cu Kα wavelength ($\lambda = 0.154059$ nm). The θ-2θ scan was carried out in 2θ range from 20° to 90° for all samples. For the AlN epilayer grown at high temperature, which had overlapping peaks of AlN and sapphire in θ-2θ scan patterns [27, 29], the ω scan was conducted at (0002) and (10-12) as well as φ scan was conducted at (10-12) of the AlN epilayers in order to estimate the crystal quality. To realize the epitaxial relationship of the AlN layer on the sapphire, the cross-section specimen of 1300 °C sample was fabricated via ion milling method, following by the TEM observation on JEOL JEM-2010. The TEM observation was also conducted to the AlN nanostructure grown at 700 °C to understand its structure.

3 Results and discussion

3.1 Morphologies and compositions of the AlN epilayer grown at high temperature

The morphologies of the AlN layer grown at 1500 °C were shown in Fig. 2. The S1 sample was dominated by specular, colorless and extreme transparent layer. Micrographs in Fig. 2a, b demonstrated its smooth surface and regular cleavage in cross-section profile respectively. According to the thickness and 30 min growth duration, the growth rate of the layer was about 50 μm/h. Moreover, there were cavities at the interface due to sapphire disassociation [30, 32, 38], as shown in Fig. 2c. The cavities helped to relax the tensile stress and suppress the cracks in the thick layer. The S2 sample had the similar smooth surface with reduced thickness of about 3 μm as the cross-section profile in Fig. 2d displayed. In contrast, the layer became discontinuous and turned into isolated islands for sample S3, as shown in Fig. 2e. It also demonstrated that large islands as well as tiny nanocone islands grew on the sapphire surface. Composition analysis by EDX spectra in Fig. 2f revealed that no discernable O was found in the layer, indicating O contamination was below the EDX detection limit (0.1 wt%).

S1 sample grown at 1300 °C was also dominated by transparent and specular layer. The epilayer had very

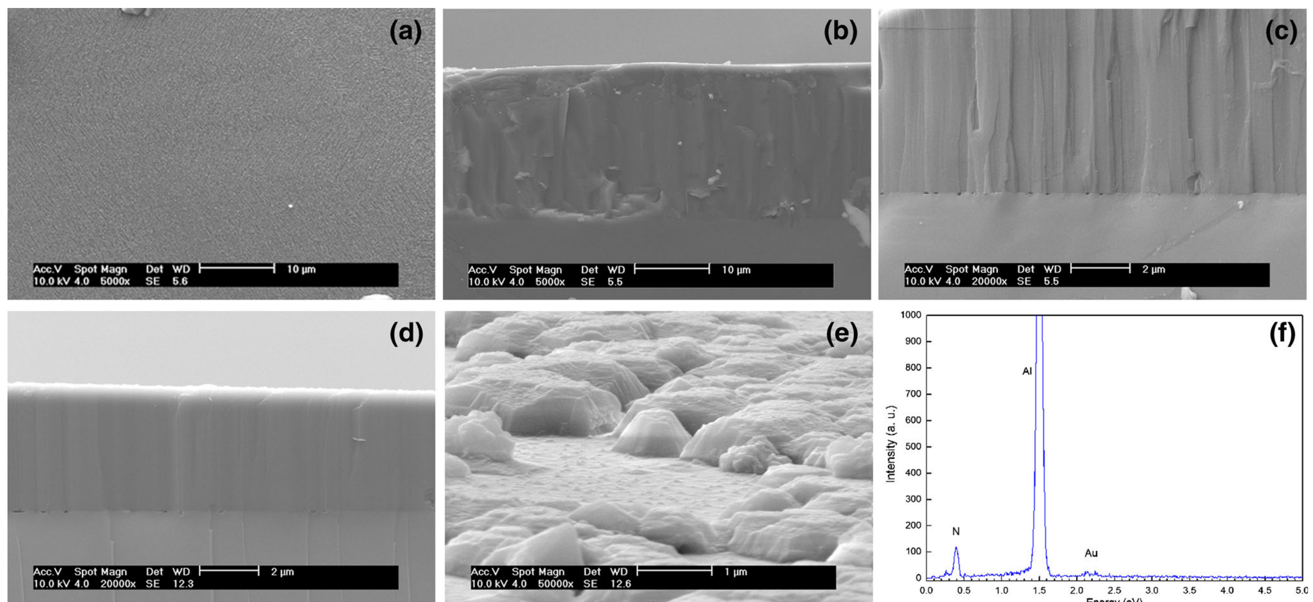

Fig. 2 Morphologies and compositions of the samples grown at 1500 °C for 30 min, **a** smooth surface of S1 sample, **b** cross-section of S1 sample, **c** regular cleavage of the layer and cavities at the interface, **d** cross-section of S2 sample, **e** isolated large islands and nanocone islands of S3 sample, **f** EDX spectra of S1 sample

smooth surface with hexagonal aligned cracks as shown in Fig. 3a. The cracks were caused by large thickness and compressive stress in the layer, which arose from mismatch of thermal expansion coefficient between the AlN layer and sapphire substrate. Enlarged view of the smooth surface in Fig. 3b revealed that the surface roughness was close to 5 nm (the size of Au particle) in the visible area (2 μm × 2.5 μm). Furthermore, there were some spiral growth and terrace structures (see Fig. 3c) at the surface. It was induced by screw dislocations originated from tilt and height difference between neighbored mosaics during coalescence [23], leading to local Frank-van der Merwe mode growth [39]. In addition, there were also domain boundaries on the surface caused by coalescence of the neighbored mosaics. According to its thickness and growth duration, the growth rate was about 50 μm/h which was equal to the growth rate at 1500 °C, in agreement with the diffusion limited growth mode [33, 40]. The enlarged view near the interface showed in Fig. 3d revealed that there were few cavities at the interface, meaning that sapphire dissociation was suppressed under 1300 °C. Meanwhile, Fig. 3d also showed that the domain boundaries generally sprouted out from the interface and extended to the layer surface, indicating that the domain boundaries did not annihilate due to low lateral growth rate in comparison with high overgrowth rate of the mosaic domain. S2 sample was also dominated by the specular, colorless and transparent appearance. As shown in Fig. 3e, the layer surface was very smooth with tiny nanopits on the layer surface. It should be pointed out that the nanopits were formed by coalescence of nanometric islands, which finally resulted in a new grew thin layer on the previous layer surface. This was in good agreement with the Stranski–Krastanov growth mode [2, 39]. The tilt view in Fig. 3f displayed that the layer thickness reduced to 2 μm.

As for the case of 1100 °C, the morphologies of S1 sample had smooth surface with hexagonal aligned domain boundaries and nanopits in large scale, as shown in Fig. 4a, b. The cross-section profile in Fig. 4c exhibited that the thickness of the layer was about 1.5 μm, indicating low growth rate of 3 μm/h. The great decline of the growth rate suggested a growth mode transition from the diffusion limited reaction to surface reaction or gas reaction limited [40].

3.2 Crystal structure and epitaxial relationship of the layer

To characterize the layers structure and estimate the crystal quality, various XRD measurements were conducted on the smooth layers surface. The sample grown at 1100, 1300 and 1500 °C had the similar XRD patterns under θ-2θ scan mode. As shown in Fig. 5a, the pattern of the 1300 °C sample displayed an overlapping pattern of sapphire (0006), AlN (0002) and (0004), indicating AlN (0002) epitaxy on c-sapphire. The φ-scan pattern of (10-12) plane of the AlN layer in Fig. 5b showed sixfold symmetry, confirming the single crystal feature of the epilayer. To evaluate the quality of the layer, ω-scan of AlN (0002) and (10-12) plane were carried out and the corresponding

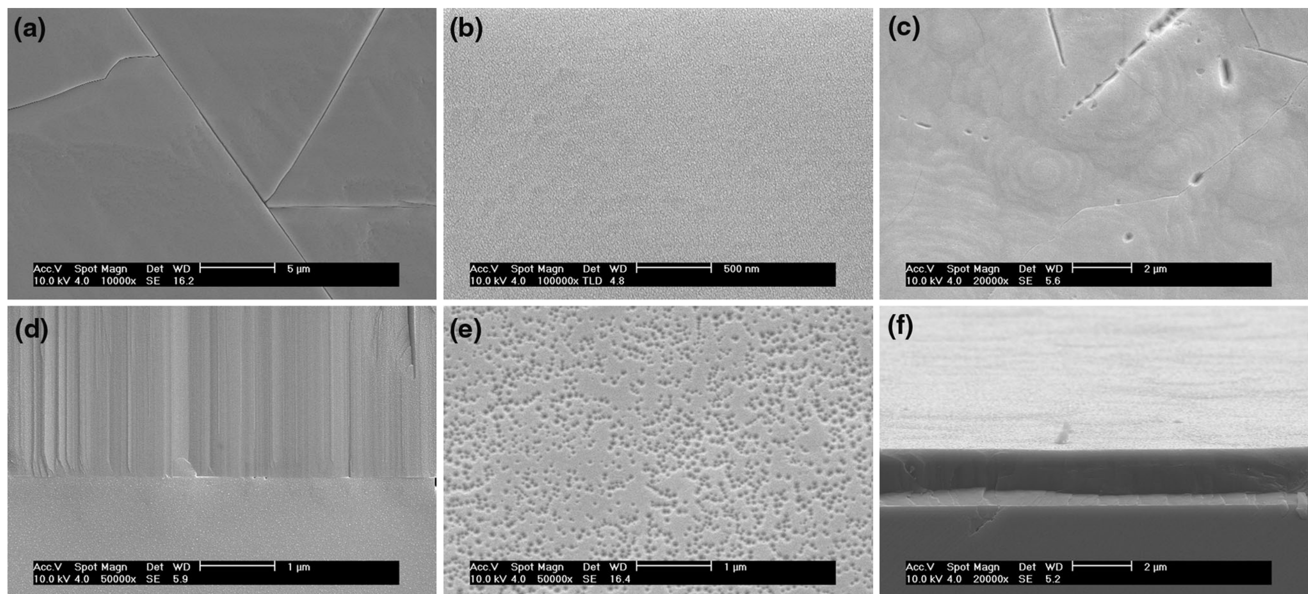

Fig. 3 Morphologies of the samples grown at 1300 °C for 50 min, **a** smooth layer surface and hexagonal aligned cracks of S1 sample, **b** enlarged view of the extreme smooth surface, **c** the spiral growth, terrace structures and hexagonal aligned domain boundaries, **d** cavity at the interface and domain boundary sprouted out from the interface, **e** smooth layer surface with nanopits of S2 sample, **f** tilt view of cross-section

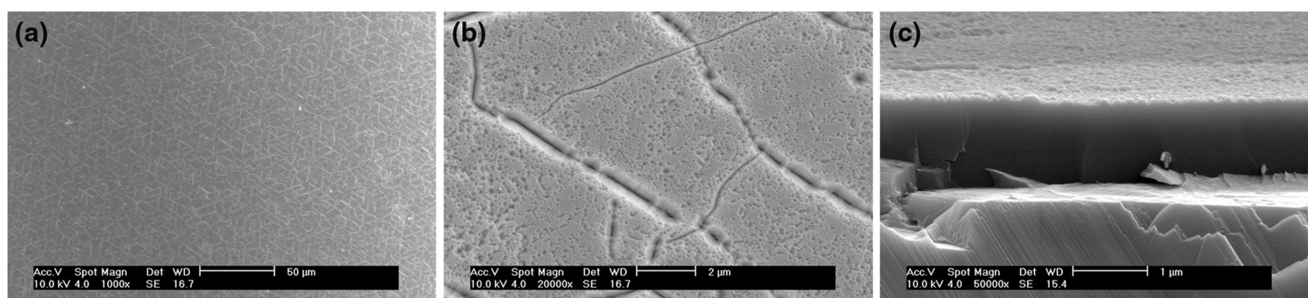

Fig. 4 Morphologies of the S1 samples grown at 1100 °C for 30 min, **a** smooth surface with hexagonal aligned domain boundaries, **b** domain boundaries and nanopits, **c** tilt view of the cross-section

rocking curves were shown in Fig. 5c, d, which revealed that the FWHM was 706 and 2754 arcsec respectively. In contrast, the FWHM of AlN (0002) was 1343 and 688 arcsec for the rocking curves of the layers grown at 1100 and 1500 °C, which was not shown. The decreasing FWHM indicated that crystal quality greatly improved at higher growth temperatures.

In order to identify the epitaxial relationship between the substrate and epilayer grown in the homebuilt HTCVD system, the cross-section specimen of the epilayer grown at 1300 °C was characterized under TEM. Bright-field TEM micrographs of the cross-section in Fig. 6a, b exhibited the threading dislocations perpendicular to the interface and nanocone islands with size of about 50 nm at the interface, in accordance with SEM image in Fig. 2e. Noteworthy, several tens of atom layers beneath the sapphire surface were substituted for AlN lattice (see Fig. 6c) due to nitridation of the substrates [41]. Figure 6d showed the HR-TEM image at the interface and the corresponding SAED pattens of the AlN layer, interface and sapphire were shown in Fig. 6e, f, g respectively. Indexing of SAED in Fig. 6d demonstrated the epitaxial relationship was AlN (0001) || sapphire (0001) with in-plane orientation relationship of AlN [1-210] || sapphire [1-100] and incidence beam parallel to [01-10]. The result was in accord with the previous MOVPE and PLD results [42, 43], which concluded with 30° rotation in the basal (0001) plane between AlN and sapphire lattice. With reference of sapphire ($c = 12.982$ angstrom), the fringe spacing between AlN (0002) plane near the interface in the HR-TEM was measured to be 2.405 angstrom (see Fig. 6d), which was slightly less than 2.489 Å (half of standard c value of

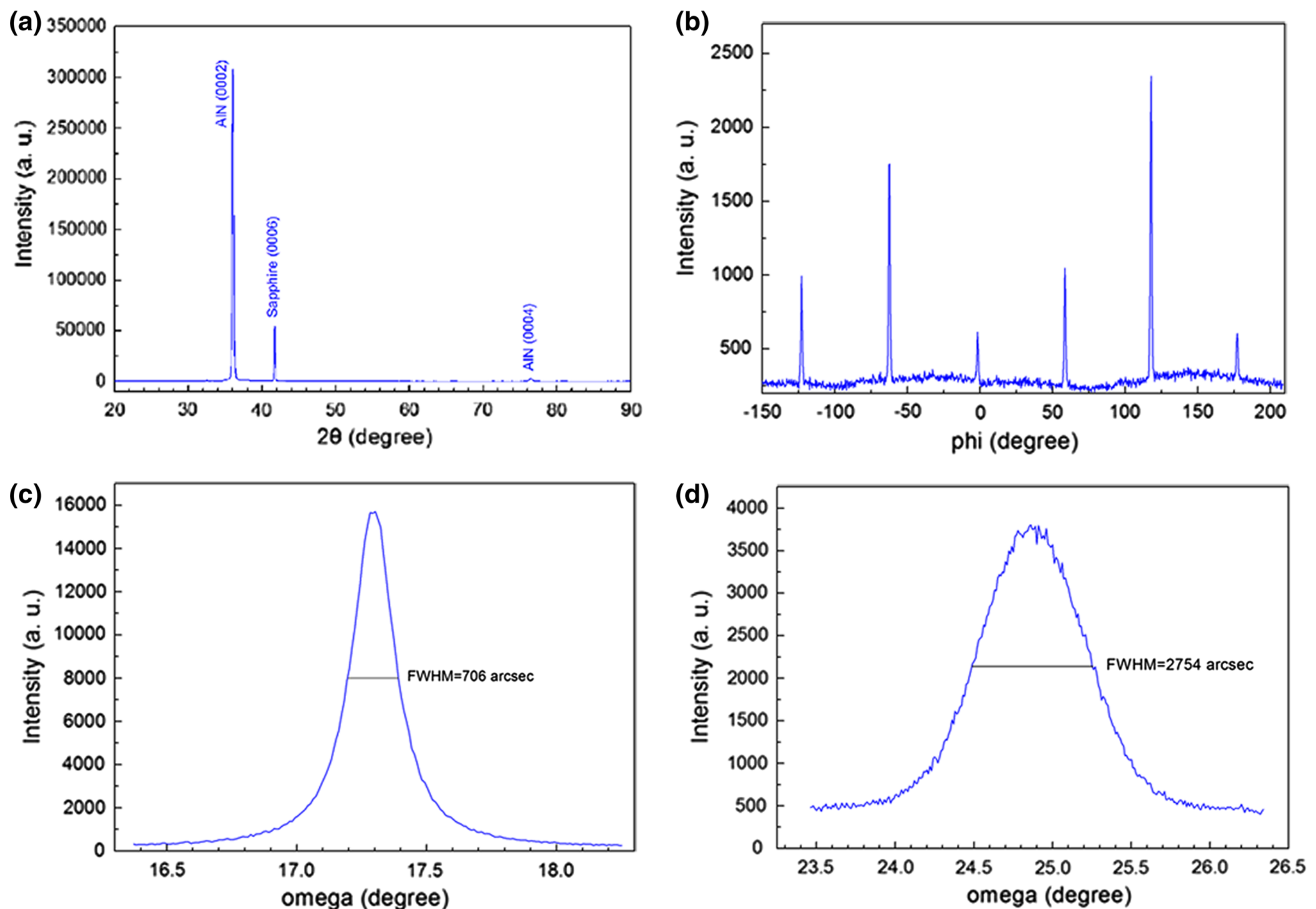

Fig. 5 XRD patterns of the sample grown at 1300 °C, **a** θ-2θ scan, **b** φ-scan pattern of (10–12) plane of the (0002) AlN layer, **c** ω-scan of AlN (0002) plane, **d** ω-scan of (10–12) plane

4.978 Å), indicating tensile stress near the interface because of lattice mismatch. On the contrary, the same spacing calculated from SAED pattern was 2.505 angstrom (see Fig. 6f) which was slightly larger than 2.489 Å, indicating compressive stress in the layer. The reason for the conflicting result was that SAED was obtained in an area larger than the range of the HR-TEM image due to the size limit of the SA aperture. In other words, the diffraction pattern brought more information from the layer far away from the interface, where the layer turned into compressive stress state during cooling stage because of the mismatch of thermal expansion coefficient between AlN layer and sapphire substrate.

3.3 Morphologies and compositions of the AlN nanostructures grown at low temperature

The sample grown at low temperature of 500, 700 and 900 °C exhibited opaque and ivory deposits, which were soft and easy to be scratched away from the substrates. Micrographs in Fig. 7a–c showed that S1 sample grown at 500 °C had rough surface which composed of aggregated sea urchin-like nanostructure with spins of 50 nm in length. There was an amorphous film with about 1 μm thickness underlaying the urchin deposits. As Fig. 7d demonstrated, S3 sample exhibited some hillocks on the flat surface of amorphous layer with 1 μm thickness instead of urchin deposits. In the case of 700 °C, the rough surface of S1 sample was also composed of urchin-like nanostructure with elongated spins of about 300 nm in length, as revealed by Fig. 7e. The surface of the S3 sample turned into nanotips array, as shown in Fig. 7f, indicating that the growth was accelerated and the amorphous layer began crystallization.

At growth temperature of 900 °C, the nanostructure on the rough surface of S1 sample turned into nanoflower, whose petal was hexagonal nanocolumn, as shown in Fig. 7g. With the increasing distance between the substrates and $AlCl_3$ nozzle, the petal of the nanoflower turned into nanorod on the surface of S3 sample, as revealed by Fig. 7h. The diameter of the nanorod increased in comparison with those produced at 500 and 700 °C. The result was in agreement with the temperature influence on

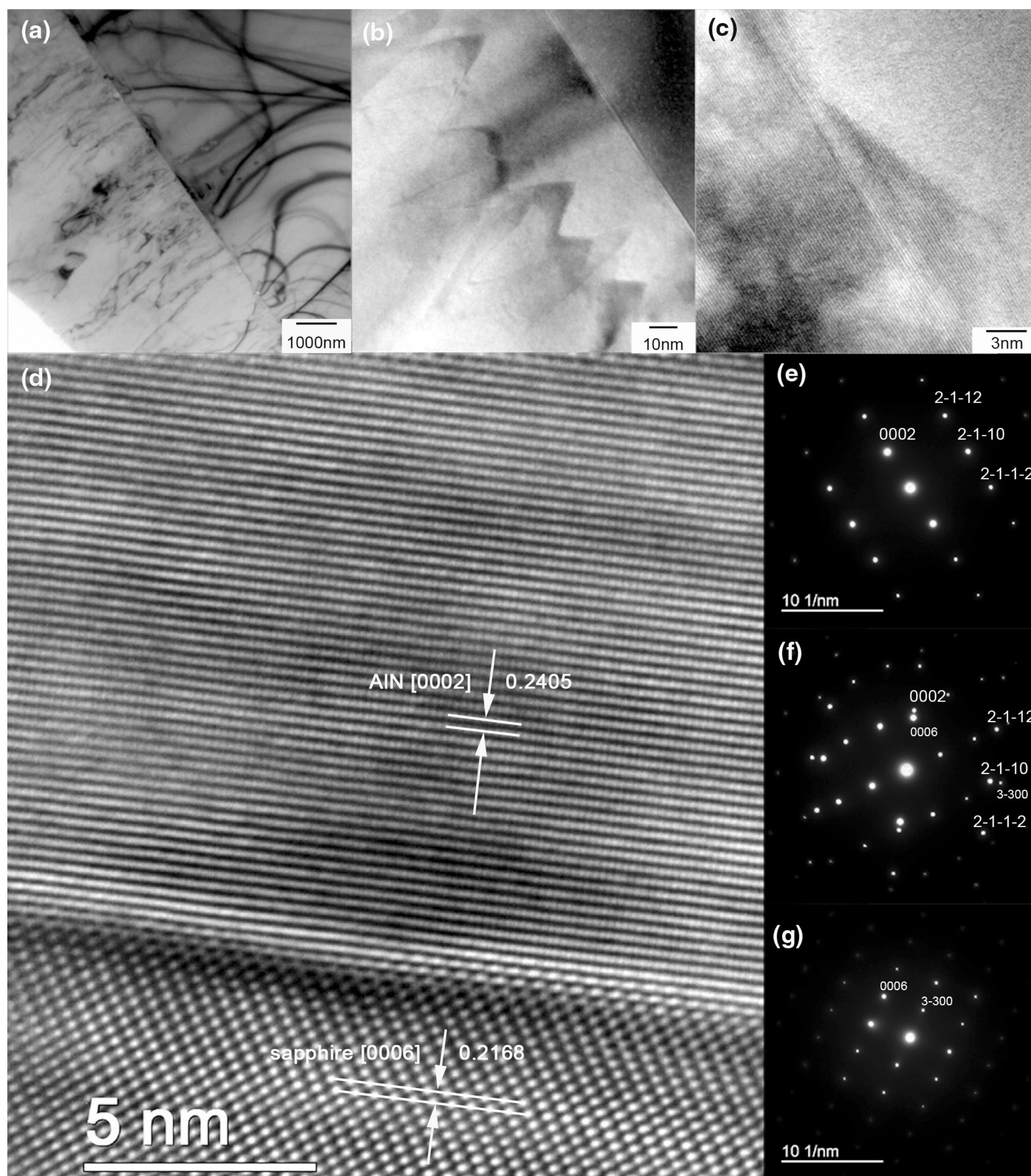

Fig. 6 TEM observation of the sample grown at 1300 °C, **a** Bright-field image of the cross-section specimen showed the threading dislocations perpendicular to the interface, **b** nanocone islands grown at the interface, **c** several tens of atom layers beneath the sapphire surface were substituted for AlN lattice, **d** HR-TEM image at the interface, **e** SAED of AlN layer, **f** SAED of interface **g** SAED of sapphire

nanotips in other researches [35–37]. Meanwhile, the diameter of the nanorod decreased with the increasing distance away from the $AlCl_3$ nozzle, i.e., with the increasing N/Al ratio due to $AlCl_3$ depletion along the flow direction. The excessive N could suppress surface diffusion and lateral growth, leading to preferred overgrowth and sharp tips [37]. That was to say that high growth temperature as well as low N/Al could promote lateral growth of the nanotip, resulting in flat and smooth top surface.

The EDX spectra of the nanostructures grown at 500, 700 and 900 °C were shown in Fig. 7i. Since the spectra were collected from the surface of S1 sample whose deposits were thick enough to prevent the signal of sapphire from being excited and detected, the O and Cl elements in the spectra should come from the deposits themselves. Meanwhile, the spectra demonstrated that O and Cl contents decreased with the increasing growth temperatures. The bonding state of Cl in AlN was not clear

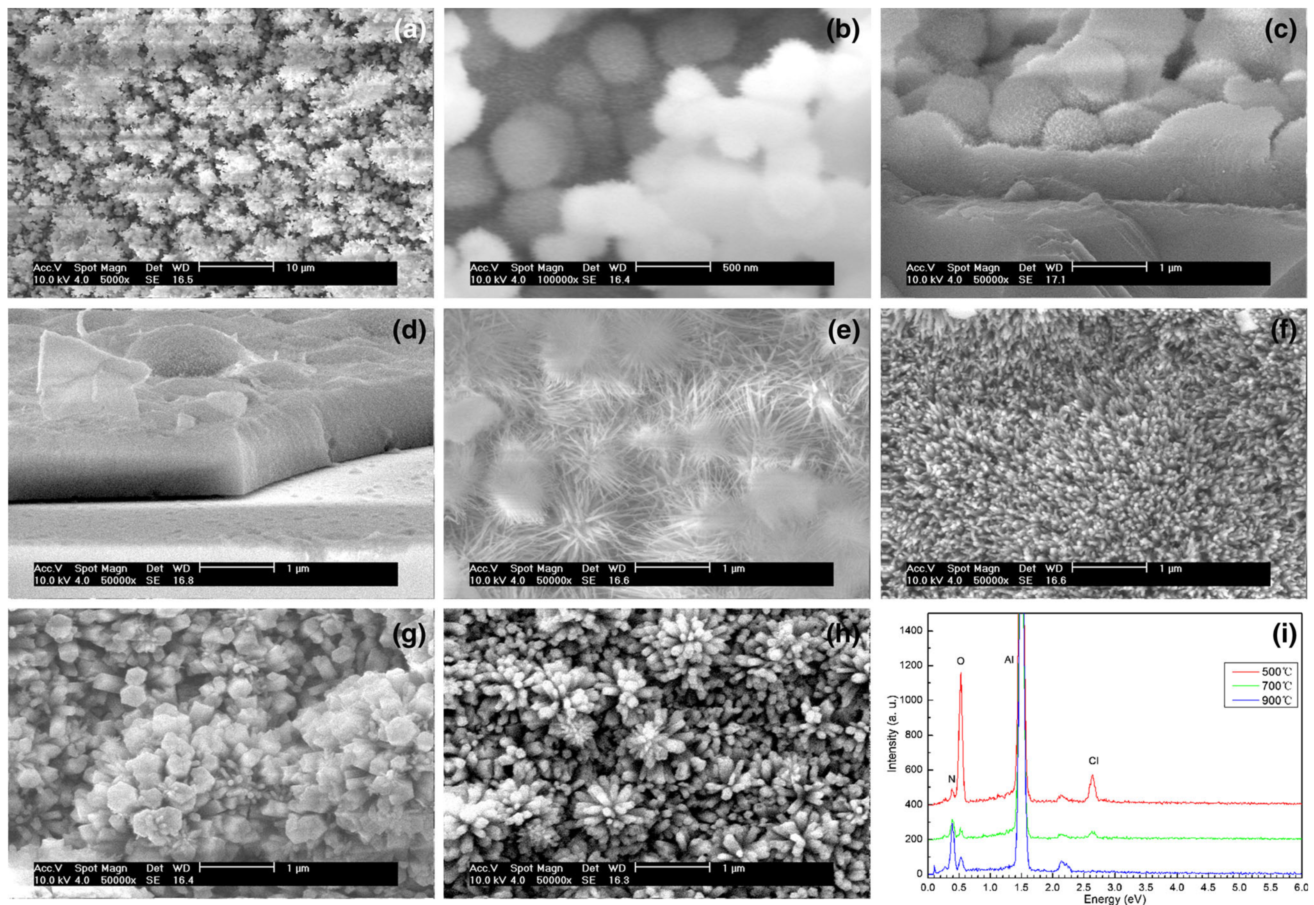

Fig. 7 Morphologies of the samples grown at low temperature, **a** rough surface of S1 sample grown at 500 °C, **b** nano urchins at the surface, **c** cross-section profile, **d** hillocks on amorphous layer of S3 sample, **e** nano urchins with elongated spins of S1 sample grown at 700 °C, **f** nanotips array of S3 sample grown at 700 °C, **g** nanoflowers assembled by nanocolumns of S1 sample grown at 900 °C, **h** nanoflowers assembled by nanorods of S3 sample, **i** EDX spectra of S1 sample grown at 500, 700 and 900 °C

till now but was suggested to be Al–Cl bond [33]. In consideration that the layers were composed of thick amorphous layer and surface nanostructures, we supposed that O and Cl should mainly originate from amorphous component of the layer rather than crystalline AlN nanostructures.

3.4 Crystal structure of the AlN nanostructures

XRD measurements were carried out in order to determine the phase and structure of the deposits. As Fig. 8a demonstrated, the XRD pattern of the deposit prepared at 500 °C had no peaks but notable amorphous hump in a wide range. It indicated that the deposit was amorphous AlN, which generally was grown at low temperature and used as buffer layer for succeeding AlN and GaN growth [29, 44, 45]. In contrast, in the case of 700 and 900 °C, the deposits dominated by crystalline AlN despite the fact that amorphous component still existed and the crystallinity of AlN was low, as demonstrated by the broadened peaks upon the amorphous hump in the patterns. In compassion with that of 700 °C case, the peaks of 900 °C case narrowed and shifted to high angle, demonstrating the crystallinity enhancement at high growth temperature. Meanwhile, we also noted that the most intensive peak transferred from (10-10) in 700 °C pattern to (0002) in 900 °C pattern, implying that c-oriented AlN growth was enhanced at 900 °C. The XRD results were in good agreement with the analysis in morphologies and compositions.

In order to observe the nanostructure in detail, TEM measurement was carried out for the nanometric sea urchin which grown at 700 °C. The low magnification image in Fig. 8b illuminated that the urchin structure was assembled by bunches of nanoneedles with 20 nm in diameter and 200 nm in length. The arcs in SAED pattern in Fig. 8c corresponded with typical textured structure feature, indicating that the nanoneedles were assembled in preferred orientation [46, 47]. This was consistent with the images in Fig. 8b, d, which displayed that the nanoneedles were

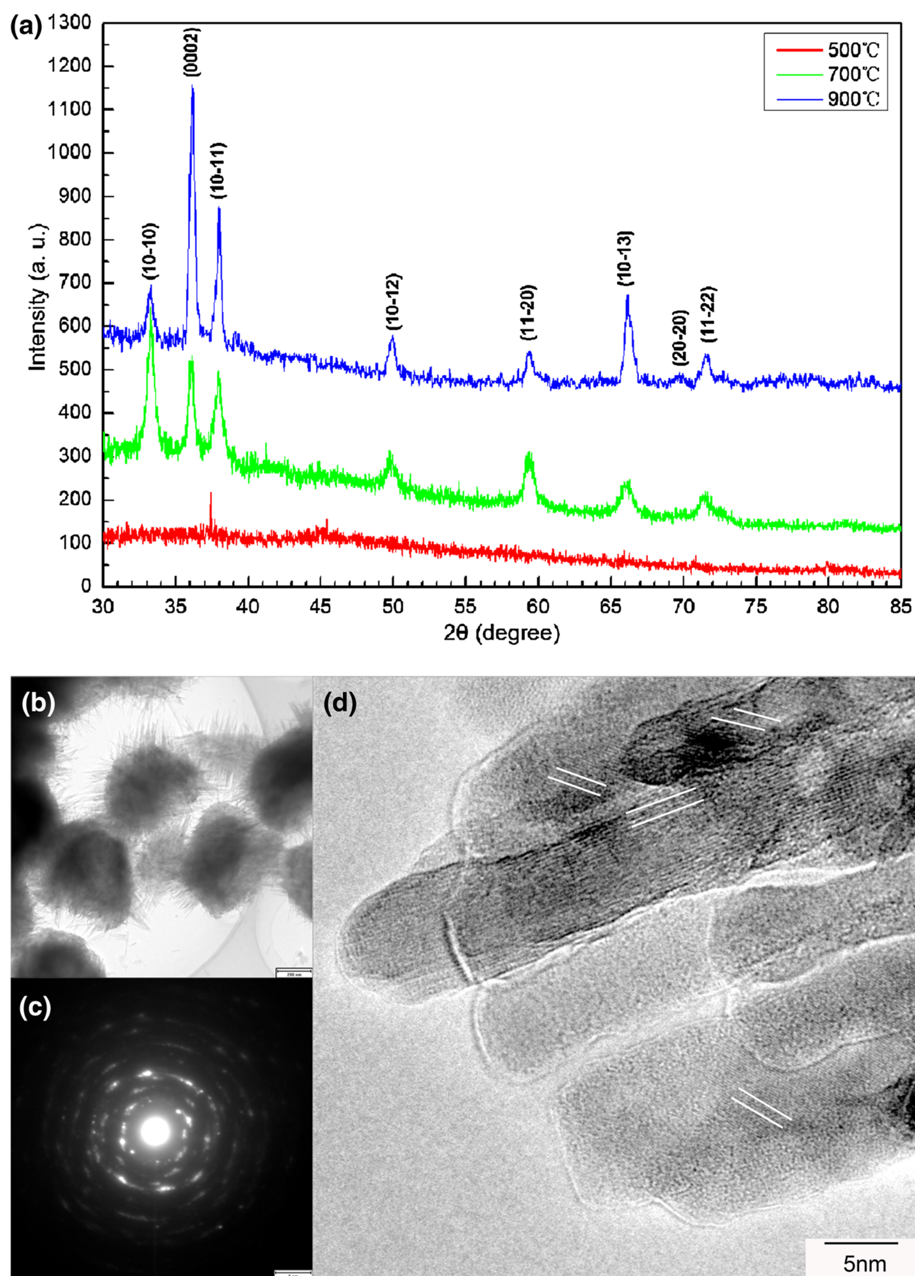

Fig. 8 Crystal structure of the nanostructure, **a** XRD patterns of the deposits grown at 500, 700 and 900 °C, **b** Bright-field image of the nano urchins grown at 700 °C, **c** SAED pattern, **d** HR-TEM image of the nanoneedles

assembled in the length direction. However, in the plane perpendicular to the length direction, the nanoneedles were arranged almost at random as revealed by the HR-TEM image in Fig. 8d, in which the directions of fringes were marked out by the white parallels. Imperfect fringes can be found in the enlarged HR-TEM image, implying the defective lattice of the AlN nano structures.

4 Conclusions

In this research, AlN were grown in wide temperature range from 500 to 1500 °C in a simple but elaborate homebuilt alumina hot-wall HTCVD system. The results showed that high quality AlN epilayers with as well as versatile AlN nanostrctures can be grown at high temperature beyond 1100 °C and low temperature below 900 °C respectively, enabling the HTCVD system to tailor various AlN structures just by changing the growth temperature. The continuous changes of morphologies and compositions of the epilayers and nanostructures illuminated that high growth temperature as well as low N/Al ratio of the atmosphere can promote surface mobility of the adatoms and lateral growth. Meanwhile, the crystal quality advancement with the increasing growth temperature was also revealed by decreasing FWHM of (0002) plane

rocking curve of the epilayer and sharpened peaks in θ-2θ XRD pattern of the nanostructures. For the AlN epilayer, its epitaixal relationship on c-sapphire was proven to be AlN (0001) || sapphire (0001) with in-plane orientation relationship of AlN [1-210] || sapphire [1-100]. Although the layer was in tensile stress state in the range of several tens of nanometers near the interface, it turned into compressive stress state out the range. Tens of atom layers of sapphire interface were substituted for AlN lattice due to nitridation. Versatile AlN nanostructures, such as sea urchin, nano flower, nanoneedle, nanorod and nanocolumn, were grown at low temperatures. Their crystal structures varied from amorphous in 500 °C case to coexistence of amorphous and defective crystalline nanourchin assembled by nanoneedles in 700 °C case, and finally to nanoflower assembled by oriented nanocolumns and nanorods with promoted crystallinity at in 900 °C case.

Acknowledgments The authors are thankful to Doc. Jing-Yi Chen who is a senior application specialist of Application Lab of PANalytical in Shanghai, China. His knowledgeable advices about characterization and skillful measurements via the HR-XRD system of Panalytical Empyrean really helped us understand the AlN layer structure.

References

1. H. Morkoc, S. Strite, G.B. Gao, M.E. Lin, B. Sverdlov, M. Burns, J Appl Phys **76**, 1363 (1994)
2. O. Ambacher, J Phys D Appl Phys **31**, 2653 (1998)
3. S. Pietranico, S. Pommier, S. Lefebvre, Z. Khatir, S. Bontemps, Microelectron Reliab **49**, 1260 (2009)
4. R.T. Bondokov, S.G. Mueller, K.E. Morgan, G.A. Slack, S. Schujman, M.C. Wood, J.A. Smart, L.J. Schowalter, J Cryst Growth **310**, 4020 (2008)
5. M.A. Moreira, I. Doi, J.F. Souza, J.A. Diniz, Microelectron Eng **82**, 802 (2011)
6. Epelbaum BM, Bickermann M, Winnacker A (2004) Second international symposium on acoustic wave devices for futrue mobile communication systems, 157
7. V. Cimalla, J. Pezoldt, O. Ambacher, J Phys D Appl Phys **40**, 6386 (2007)
8. D. Dharanipal, R. Mlcak, J. Chan, H.L. Tuller, J. Abell, W. Li, T.D. Moustaka, Proc Electrochem Soc PV **6**, 287 (2004)
9. Y. Taniyasu, M. Kasu, T. Makimoto, Nature **441**, 325 (2006)
10. S. Nikishin, B. Borisov, V. Kuryatkov, M. Holtz, A. Gregory, Wendy L. Sarney, Anand V. Sampath, H. Shen, M. Wraback, A. Usikov, V. Dmitriev, J Mater Sci Mater Electron **19**, 764 (2008)
11. H. He, L. Huang, M. Xiao, F. Yuechun, X. Shen, J. Zeng, J Mater Sci Mater Electron **24**, 4499 (2013)
12. A. Kakanakova-Georgieva, R.R. Ciechonski, U. Fosberg, A. Lundskog, E. Janzén, Cryst Growth Des **9**, 880 (2009)
13. M. Bickermann, B.M. Epelbaum, O. Filip, P. Heimann, M. Feneberg, S. Nagata, A. Winnacker, Phys Status Solidi C **7**, 1743 (2010)
14. V.N. Jmerik, A.M. Mizerov, D.V. Nechaev, P.A. Aseev, A.A. Sitnikova, S.I. Troshkov, P.S. Kop'ev, S.V. Ivanov, J Cryst Growth **354**, 188 (2012)
15. H. Okumura, T. Kimoto, J. Suda, Appl Phys Exp **5**, 1055021 (2012)
16. A. Kakanakova-Georgieva, D. Nilsson, E. Janzén, J Cryst Growth **338**, 52 (2012)
17. X. Chen, S. Li, J. Kang, J Mater Sci Mater Electron **19**, S215 (2008)
18. http://www.hexatechinc.com/
19. L.J. Schowalter, S.B. Schujman, W. Liu, M. Goorsky, M.C. Wood, J. Grandusky, F. Shahedipour-Sandvik, Phys Status Solidi a **203**, 1667 (2006)
20. M. Bichermann, O. Filip, B.M. Epelbaum, P. Heimann, M. Feneberg, B. Neuschl, K. Thonke, E. Wedler, A. Winnacker, J Cryst Growth **339**, 13 (2012)
21. H. Matsubara, K. Mizuno, Y. Takeuchi, S. Harada, Y. Kitou, E. Okuno, T. Ujihara, Jpn J Appl Phys **52**, 08JE17 (2013)
22. M. Yonenura, K. Kamei, S. Munetoh, J Mater Sci Mater Electron **16**, 197 (2005)
23. A. Volkova, V. Ivantsov, L. Leung, J Cryst Growth **314**, 113 (2011)
24. Y. Katagiri, S. Kishino, K. Okuura, H. Miyake, K. Hiramatu, J Cryst Growth **311**, 2831 (2009)
25. Y. Kumagai, T. Yamane, A. Koukitu, J Cryst Growth **28**, 162 (2005)
26. T. Nagashima, M. Harada, H. Yanagi, Y. Kumagai, J Cryst Growth **300**, 42 (2007)
27. Derrick Shane Kamber (2008) Hydride Vapor Phase Epitaxy of Aluminum Nitride, Dissertation, University of California Santa Barbara
28. K.-i. Eriguchi, H. Murakami, U. Panyukova, Y. Kumagai, S. Ohira, A. Koukitu, J Cryst Growth **298**, 332 (2007)
29. K.-i. Eriguchi, T. Hiratsuka, H. Murakami, Y. Kumagai, A. Koutitu, J Cryst Growth **310**, 4016 (2008)
30. D.F. Bliss, V.L. Tassev, D. Weyburne, J.S. Bailey, J Cryst Growth **250**, 1 (2003)
31. J. Tajima, H. Murakami, Y. Kumagai, K. Takada, A. Koukitu, J Cryst Growth **311**, 837 (2009)
32. W. Jie-Jun, Y. Katagiri, K. Okuura, D.-B. Li, H. Miyake, K. Hiramatsu, J Cryst Growth **311**, 3801 (2009)
33. A. Dollet, Y. Casaux, G. Chaix, C. Dupuy, Thin Solid Films **406**, 1 (2002)
34. J. Yang, T.-W. Liu, C.-W. Hsu, L.-C. Chen, K.-H. Chen, C.-C. Chen, Nanotechnology **17**, S321 (2006)
35. F. Zhang, Q. Wu, X. Wang, N. Liu, J. Yang, Vacuum **86**, 833 (2012)
36. Y. Gao, H. Mingzhe, C. Xiangcheng, Y. Qingfeng, J Mater Sci Mater Electron **24**, 4008 (2013)
37. X. Song, Z. Guo, J. Zheng, L. Xingguo, Y. Pu, Nanotechnology **19**, 1156091 (2008)
38. Y. Kumagai, Y. Enatsu, M. Ishizuki, Y. Kubota, J. Tajima, T. Nagashima, H. Murakami, K. Takada, A. Koukitu, J Cryst Growth **312**, 2530 (2010)
39. T.D. Moustakas, S.E. Mohney, S.J. Pearton, Proceedings of the third symposium on III–V nitride materials and processes. Electrochemical Soc **98**, 130 (1999)
40. H. Komiyama, Y. Shimogaki, Y. Egashira, Chem Eng Sci **54**, 1941 (1999)
41. F. Dwikusuma, T.F. Kuech, J Appl Phys **94**, 5656 (2003)
42. Sarad Bahadur Thapa (2010) Studies of AlN grown by MOVPE for electronic and optoelectronic applications. Dissertation, Ulm University
43. R.D. Vispute, H. Wu, J. Narayan, Appl Phys Lett **67**, 1549 (1995)
44. M. Iwaya, T. Takeuchi, S. Yamaguchi, C. Wetzel, H. Amano, I. Akasaki, Jpn J Appl Phys **37**, 316 (1998)
45. D.G. Zhao, J.J. Zhu, Z.S. Liu, S.M. Zhang, H. Yang, D.S. Jiang, Appl Phys Lett **85**, 1449 (2004)
46. R.A. Schwarzer, Texture Microstruct **20**, 7 (1993)
47. David B, Williams C, Barry Carter (2009) Transmission electron microscopy, A textbook for materials science (2009, Springer Science + Business Media, New York), p. 290